PERGAMON

International Journal of Heat and Mass Transfer 43 (2000) 993–1005

International Journal of HEAT and MASS TRANSFER

www.elsevier.com/locate/ijhmt

Temperature decay in two-phase turbulent flows

F.A. Jaberi [a,*], F. Mashayek [b]

[a] Department of Mechanical and Nuclear Engineering, Kansas State University, Manhattan, KS 66506-5205, USA
[b] Department of Mechanical Engineering, University of Hawaii at Manoa, 2540 Dole Street, Honolulu, HI 96822, USA

Received 10 September 1998; received in revised form 7 May 1999

Abstract

Direct numerical simulations of dilute two-phase flows are conducted to study the decay of the fluid and particle temperatures in isotropic turbulence. Both one-way and two-way coupling between phases are considered. The effects of the particle response time (τ_p), the Prandtl number (Pr), the ratio of specific heats (α), and the mass loading ratio (ϕ_m) on the carrier fluid and particle temperature statistics are studied. The results indicate that the variance of the fluid and particle temperatures, the dissipation rate of the fluid temperature and the high wavenumber values of the fluid temperature spectrum are increased as the magnitudes of ϕ_m and/or αPr increase. The decay rate of the fluid and particle temperature variances are similar when the values of αPr are small. For large αPr values, the variance of the particle temperature is higher than that of the fluid and is strongly dependent on the initial conditions. The Lagrangian auto-correlation coefficient of the particle temperature (R_T^p) also behaves differently for different magnitudes of α and Pr. For small values of α, R_T^p decreases as the magnitude of particle response time increases. For large values of α, R_T^p increases with increasing τ_p.

Keywords: Two-phase turbulent flows; Thermal transport; Direct numerical simulations

1. Introduction

One of the most interesting aspects of turbulent fluid motion is the enhanced diffusion of scalar quantities suspended in it [1–3]. These scalars may be light tracer particles or chemical species which are able to follow the turbulent velocity fluctuations or they may be heavy particles or droplets which cannot completely follow the carrier fluid velocity because of their finite inertia. This aspect of turbulent diffusion, i.e heavy particle dispersion, is more complicated due to additional parameters that enter into the problem [4–10]. Prediction of particle-laden turbulent flows is, however, very important since these flows occur frequently in nature and in industry. Flows in energy conversion devices (such as spray combustion) or turbulent dispersion of pollutants in atmosphere being two examples.

Owing to extensive previous studies, much is known about the particle dispersion and the statistics of the fluid and particle velocities in two-phase turbulent flows. However, our knowledge about the thermal transport between the phases and the particle/fluid temperature statistics is very limited. This is mainly due to lack of sufficient experimental data [11–13]. An approach which provides reliable data and does not suffer from the difficulties of the 'Lagrangian particle

* Corresponding author. Tel.: +1-785-532-5619; fax: +1-785-532-7057.
E-mail address: jaberi@mne.ksu.edu (F.A. Jaberi).

0017-9310/00/$ - see front matter
PII: S0017-9310(99)00185-4

Nomenclature

C_D	drag coefficient
d_p	particle diameter
F_i	velocity forcing function
k	magnitude of the Fourier wavenumber
m_p	particle mass
Nu	Nusselt number
N_p	total number of particles
Pr	Prandtl number
p	pressure
R_T^p	auto-correlation coefficient of the particle temperature
Re_0	reference Reynolds number
Re_p	particle Reynolds number
Re_λ	Taylor micro-scale Reynolds number
S_H	heat source term
S_{Mi}	ith component of the momentum source term
t	time
t_D	the time normalized by the Eulerian integral time scale
T	fluid temperature
T_p	particle temperature
u_i	ith component of the fluid velocity **U**
v_i	ith component of the particle velocity **V**
X_i	Lagrangian coordinates
x_i	Eulerian coordinates
α	ratio of the specific heat of the particle to that of the fluid
ϵ	dissipation rate of the turbulent kinetic energy
ϵ_T	dissipation rate of the fluid temperature
η	Kolmogorov length scale
ρ	fluid density
ρ_p	particle density
τ_k	Kolmogorov time scale
τ_l	Eulerian integral time scale
τ_p	particle response time
ϕ_m	mass loading ratio

property measurements' is the method of direct numerical simulation (DNS). In DNS, all the fluctuations of the carrier fluid is resolved and the particles are traced in a Lagrangian manner. Therefore, the instantaneous fluid and particle fields are 'fully' known. Although DNS has been extensively used for two-phase flows [14–16], its application to the study of thermal transport between phases is very limited. In a recent study, Jaberi [17] examines the temperature statistics in homogeneous two-phase turbulent flows via DNS. In this study,both the velocity and the temperature fields are set to be statistically stationary via forcing of the large scale fluid velocity and temperature fields. The results of this study are consistent with the theoretical results of Yarin and Hetsroni [13] and indicate that the stationary value of the particle temperature intensity is a decreasing function of the particle time constant τ^p, the Prandtl number Pr, the ratio of the specific heats, and the flow Reynolds number Re_λ. It has also been found that the auto-correlation coefficient of the particle temperature (R_T^p) exhibits behavior different than that of the particle velocity (R_v^p) and is not significantly dependent on the magnitudes of τ_p, Pr and when the values of αPr and/or τ_p are small. For higher values of αPr and/or τ_p, R_T^p increase noticeably with τ_p, Pr and α. Additionally, the fluid and particle statistics have shown to be affected by the particles, more so for higher particle mass loading ratio, ϕ_m. Selective modification of the turbulence by small size particles results in significant attenuation of enstrophy production. Therefore, the magnitude of the velocity derivative skewness decreases when ϕ_m increases. The results also indicate that with increasing the mass loading, the coupling between the fluid temperature and its dissipation enhances. The ratio of particle to fluid temperature intensities and the dissipation of fluid temperature fluctuations decrease as ϕ_m increases.

The previous DNS studies suggest that the response of particle velocity to fluid velocity and also the modification of fluid velocity by particles in decaying turbulence are different from those in stationary turbulence. Similarly, we expect that the statistical behavior of the fluid and particle temperatures to be dependent on the flow stationary (or lack thereof). It is, therefore, instructive to examine the temperature statistics when the temperature field or more precisely its turbulent fluctuations decay. A similar study may also be done in laboratory and experimental assessment of the temperature decay in two-phase grid-generated turbulence is in order. This work is an extension of that by Jaberi [17], and consider the response of particle temperature to the decay of the carrier fluid temperature, and also the modification of fluid temperature field by particles for different flow and particle parameters.

2. Governing equations and computational methodology

The transport of the carrier fluid velocity and temperature are treated in the Eulerian frame of reference and are governed by the continuity, momentum and

energy equations which include the particle source terms. By assuming small variations for the fluid velocity, pressure, temperature, and with the assumption of constant thermodynamic properties, the normalized form of the carrier fluid equations are expressed as:

$$\frac{\partial u_j}{\partial x_j} = 0 \tag{1}$$

$$\frac{\partial u_i}{\partial t} + \frac{\partial (u_i u_j)}{\partial x_j} = -\frac{\partial p}{\partial x_i} + \frac{1}{Re_0}\frac{\partial^2 u_i}{\partial x_j \partial x_j} + F_i + S_{\mathrm{M}} \tag{2}$$

$$\frac{\partial T}{\partial t} + \frac{\partial (u_j T)}{\partial x_j} = \frac{1}{Re_0 Pr}\frac{\partial^2 T}{\partial x_j \partial x_j} + S_{\mathrm{H}} \tag{3}$$

where u_i is the fluid velocity in x_i direction, p and T are fluid pressure and temperature respectively, and t represents time. The modification of the carrier fluid by particles is expressed through the momentum (S_{M}) and heat (S_{H}) source terms. The mathematical definition and the physical significance of these source terms are expressed below. To keep the fluid velocity stationary, in some cases, the low wavenumber spectral values of velocity spectrum are randomly forced via an isotropic and solenoidal stochastic forcing function, F_i [17–19]. The forcing function is described in detail by Eswaran and Pope [19]. All variables in the above equations are normalized using reference length (L_0), velocity (U_0), temperature (T_0) and density (ρ_0) scales (the non-dimensional density is unity). Consequently, the two important non-dimensional parameters are the Reynolds number ($Re_0 = \frac{\rho_0 U_0 L_0}{\mu}$, μ is the fluid viscosity) and the Prandtl number (Pr).

The particle equations are derived based on assumptions that the particles are fine and heavy, and the mixture is dilute. Therefore, particle collisions are infrequent and are ignored. The transport properties of a single spherical particle in non-uniform flows have been extensively studied in the past [20–22]. For the range of particle Reynolds numbers considered here, it is adequate to use the modified Stokes relations for the particle transport coefficients [23,24]. The acceleration of particles due to forces other than the drag force and also the heat transfer by means other than the 'steady-state' convection are ignored. Consequently, the evolution of the particle displacement vector (X_i), the velocity vector (v_i), and the temperature (T_{p}) are governed by the following equations:

$$\frac{\mathrm{d}X_i}{\mathrm{d}t} = v_i \tag{4}$$

$$\frac{\mathrm{d}v_i}{\mathrm{d}t} = \frac{C_{\mathrm{D}} Re_{\mathrm{p}}}{24\tau_{\mathrm{p}}}\left(u_i^* - v_i\right) \tag{5}$$

$$\frac{\mathrm{d}T_{\mathrm{p}}}{\mathrm{d}t} = \frac{Nu}{3\alpha Pr\tau_{\mathrm{p}}}\left(T^* - T_{\mathrm{p}}\right) \tag{6}$$

where the asterisk (*) refers to the local fluid variables which are interpolated to the particle position, and α is the ratio of the specific heat of the particle to constant pressure specific heat of the fluid. The non-dimensional particle time constant (τ_{p}) is;

$$\tau_{\mathrm{p}} = \frac{Re_0 \rho_{\mathrm{p}} d_{\mathrm{p}}^2}{18} = \frac{\rho_{\mathrm{p}}^{1/3} Re_0}{18}\left(\frac{6m_{\mathrm{p}}}{\pi}\right)^{2/3} \tag{7}$$

where ρ_{p}, d_{p} and m_{p} are the particle density, diameter and mass, respectively. The magnitude of ρ_{p} is 1000. The particle drag coefficient (C_{D}), the Reynolds number (Re_{p}) and the Nusselt number (Nu) in modified Stokes relations are expressed by

$$C_{\mathrm{D}} = \frac{24\left(1 + 0.15 Re_{\mathrm{p}}^{0.687}\right)}{Re_{\mathrm{p}}} \tag{8}$$

$$Re_{\mathrm{p}} = Re_0 \rho^* d_{\mathrm{p}} |u_i^* - v_i| \tag{9}$$

$$Nu = 2 + 0.6 Re_{\mathrm{p}}^{0.5} Pr^{0.33} \tag{10}$$

The volumetric source terms in fluid momentum and heat equations (S_{M} and S_{H}) are evaluated based on the discrete particle-source-in-cell (PSIC) model of Crowe et al. [23] and are expressed as;

$$S_{\mathrm{M}} = -\frac{1}{\Delta V}\sum\left\{m_{\mathrm{p}}\frac{\mathrm{d}v_i}{\mathrm{d}t}\right\} = -\frac{1}{\Delta V}\sum\left\{\frac{C_{\mathrm{D}} Re_{\mathrm{p}} m_{\mathrm{p}}}{24\tau_{\mathrm{p}}}\left(u_i^* - v_i\right)\right\} \tag{11}$$

$$S_{\mathrm{H}} = -\frac{1}{\Delta V}\sum\left\{\alpha m_{\mathrm{p}}\frac{\mathrm{d}T_{\mathrm{p}}}{\mathrm{d}t}\right\} = -\frac{1}{\Delta V}\sum\left\{\frac{Num_{\mathrm{p}}}{3Pr\tau_{\mathrm{p}}}\left(T^* - T_{\mathrm{p}}\right)\right\}, \tag{12}$$

where the summation is taken over all particles in the volume $\Delta V = (\Delta x)^3$ (Δx is the grid spacing) centered at each Eulerian (grid) point. These Eulerian source terms are obtained from the Lagrangian particle fields by localized volume averaging. The momentum source term, S_{M} represents the momentum transfer between the phases due to particle drag force. The heat source term represents the exchange of the internal energy by convective heat transfer.

The particles, in general, can exchange mass, momentum and energy (both internal and kinetic) with the carrier fluid, resulting in a very complicated two-way interaction between the phases. For fine, heavy

and non-evaporative/non-reactive particles in dilute mixture, the particles affect the carrier fluid (an vice versa) due to momentum and heat transfer between the phases. The momentum transfer is due to deforming effect of the drag force on the surrounding fluid element and also due to direct acceleration (or deceleration) of the carrier fluid via particle drag force. The former is neglected in our constant density analysis and the later is represented by S_M. The energy transfer involves the changes in both the internal energy and kinetic energy of the fluid and particles. The variation in fluid turbulent kinetic energy, as explained in several previous studies, is due to particle drag and can be quantified by using the momentum Eq. (2). The fluid internal energy is changed due to molecular viscous dissipation at small scales and due to direct energy transfer between the fluid and the particles via thermal convection and radiation. In the derivation of Eqs. (3) and (12), the heat generated by the viscous dissipation of the turbulent motions and also that due to particle drag force are neglected. The radiation heat transfer are also neglected as the variations in temperature are small. Consequently, S_H is the only heat source term in the carrier fluid temperature Eq. (3).

The transport equations of the fluid mass, momentum and heat (Eqs. (1)–(3)) are integrated using the Fourier pseudo-spectral method [25] with triply periodic boundary conditions. Aliasing errors are treated by truncating the Fourier values outside the shell with wavenumber $k_{max} = \sqrt{2}N/3$ (where N is the number of grid points in each direction). The explicit second order accurate Adams–Bashforth scheme is used to time advance the variables in the Fourier space. All simulations are conducted within a box containing 96^3 collocation points. The magnitudes of the flow Reynolds and Prandtl numbers vary for different cases but are selected in such a way that the resolution of small scales is guaranteed. This is accomplished by keeping the magnitude of ηk_{max} (η is the Kolmogorov length scale) greater than 1.47 [26,18,27].

The particle momentum and heat transfer equations (Eqs. (5) and (6)) and the particle trajectory equation (Eq. (4)) are integrated using the second order Adams–Bashforth scheme. In order to evaluate fluid quantities at the particle locations a fourth-order accurate Lagrangian interpolation scheme is employed. The number of particles varies in different simulations but it is never less than 28^3. This number of particles is enough to calculate the particle statistics with less than 1% error. In the discussion of the results below $\langle\langle\ \rangle\rangle$ denotes the Lagrangian average taken over ensembles of particle or fluid elements. The Eulerian ensemble average is denoted by $\langle\ \rangle$ and is conducted over all the collocation points. The flow Reynolds number (Re_λ) is defined, based on the Taylor micro length scale (λ) and

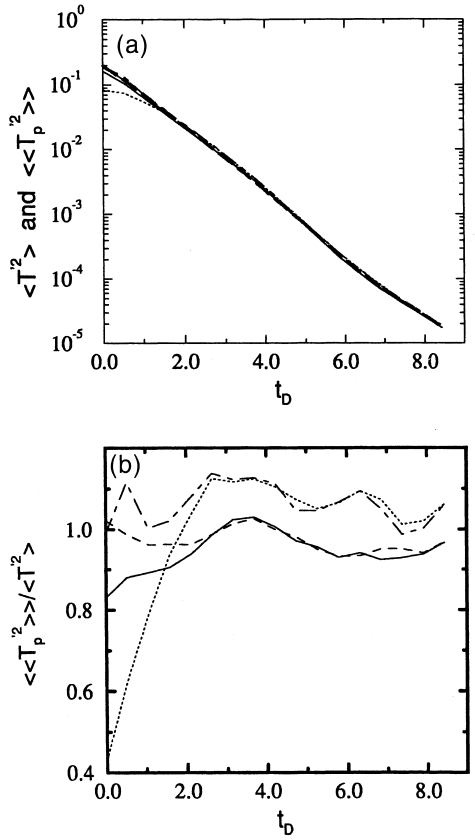

Fig. 1. Temporal variation of (a) the particle and fluid temperature variances and; (b) their ratio. For all cases, $\alpha = 1$ and $Pr = 0.7$. Solid line denotes $\langle\langle T_p'^2\rangle\rangle$ or $\frac{\langle\langle T_p'^2\rangle\rangle}{\langle T'^2\rangle}$ for $\frac{\tau_p}{\tau_k} = 0.5$ and stationary initial condition; dashed line for $\frac{\tau_p}{\tau_k} = 0.5$ and random initial condition; dotted line for $\frac{\tau_p}{\tau_k} = 7$ and stationary initial condition, and dashed–dotted line for $\frac{\tau_p}{\tau_k} = 7$ and random initial condition. The thick dashed line represents $\langle T'^2\rangle$.

the turbulence intensity ($\frac{1}{3}\langle u_i u_i\rangle$). The 'prime' denotes the mean subtracted quantity and ϕ_m is the mass loading ratio.

3. Temperature decay in stationary turbulence

In this section, we investigate one-way and two-way interactions between phases for decaying temperature field while the velocity field is stationary. The velocity is initialized as a random, solenoidal, and three-dimensional (3D) field with zero mean and a Gaussian spectral density function. This field is artificially forced by the function F_i to yield a stationary and 'self-similar' turbulent flow. In stationary turbulence, the long time values of the particle and fluid velocity statistics are independent of initial conditions and are characterized

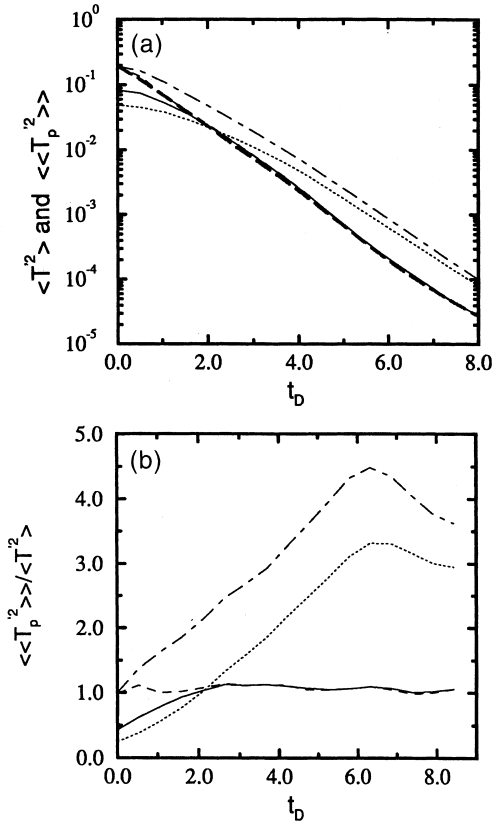

Fig. 2. Temporal variation of (a) the particle and fluid temperature variances and, (b) their ratio. For all cases, $\tau_p = 3.6$ and $Pr = 0.7$. Solid line represents the case with $\alpha = 0.25$ and stationary initial condition; dashed line for $\alpha = 0.25$ and random initial condition; dotted line for $\alpha = 4$ and stationary initial condition; dotted–dashed line for $\alpha = 4$ and random initial condition.

by the fluid and particle parameters (i.e. τ_p, ϕ_m and Re_λ). In all cases considered below, the initial fluid velocity and temperature fields are similar to those of Jaberi [17] with $Re_\lambda = 47.2$, $\langle T'^2 \rangle = 0.193$ and $Pr = 0.7$.

3.1. One-way coupling

It has been found in the previous studies [27,28] that the statistical evolution of decaying temperature field in single-phase homogeneous turbulent flows is dependent on the initial conditions. This suggests that the particle temperature statistics might also be dependent on the initial flow and particle conditions. To examine this dependency, in Fig. 1(a), the decay of the particle and fluid temperature variances ($\langle\langle T'^2_p \rangle\rangle$ and $\langle T'^2 \rangle$) for different particle inertia and for two different initial particle conditions are considered. Particles with 'random' initial condition are randomly distributed in space and have the same velocity and temperature as the surrounding fluid. The initial positions, velocities and temperatures of the particles with 'stationary' initial condition are the same as those of the stationary fields considered in Ref. [17]. For all cases, $\alpha = 1$ and $Pr = 0.7$. Fig. 1(a) shows that after a transient time, the effects of particle initial condition diminish and particles with random and stationary initial conditions adopt the same temperature variance. It is also observed that regardless of the magnitude of particle response time, the values of the particle and fluid temperature variances are very close. This indicates that the response time of the particle temperature (to the variations in fluid temperature) is smaller than the time scale associated with the decay of temperature fluctuations. The difference between the particle and fluid temperature fields is better shown in Fig. 1(b), where the temporal variation of $\frac{\langle\langle T'^2_p \rangle\rangle}{\langle T'^2 \rangle}$ is considered. The results in this figure indicate that for all cases the long time values of $\frac{\langle\langle T'^2_p \rangle\rangle}{\langle T'^2 \rangle}$ are statistically stationary and close to unity. However, the early time values deviate significantly from unity when particles are heavy (τ_p is large) and start with stationary conditions. After the early transient time, $\frac{\langle\langle T'^2_p \rangle\rangle}{\langle T'^2 \rangle}$ is only dependent on the particle response time. Particles with small inertia have slightly lower temperature variance than those of the fluid, but particles with large inertia have slightly higher variances.

The results shown in Fig. 2 for $\alpha = 0.25$ are similar to those in Fig. 1, indicating that the long time values of $\frac{\langle\langle T'^2_p \rangle\rangle}{\langle T'^2 \rangle}$ are almost constant, close to unity and independent of initial conditions. We, therefore, conclude that the behavior observed in Fig. 1 is valid for all values of α as long as α is close to or less than unity. However, the evolution of the particle statistics is different for larger α values. Particles with large heat capacity (large α values)respond slowly to the decay of carrier fluid temperature fluctuations. Therefore, their temperature intensity remains higher than that of the fluid. This is observed in Fig. 2, where it is shown that for $\alpha = 4$ the decay rate of the particle temperature variance is less than that of the carrier fluid and the long time values of $\frac{\langle\langle T'^2_p \rangle\rangle}{\langle T'^2 \rangle}$ are substantially larger than unity. Additionally, the effects of initial conditions become more important as the magnitude of α increases. Fig. 2 shows that for $\alpha = 4$ the effects of initial particle temperature remain significant even after eight eddy turn-over times. This is an important observation and suggests that in two-phase reacting flows the reaction rate is strongly dependent on the initial (inlet) particle temperature conditions when α is large. A similar behavior is expected for large Prandtl numbers. Despite the differences in variances, the shape of the probability density functions (pdf) of the fluid and particle temperatures remain close to a normal (Gaussian) distribution in all cases and at all times.

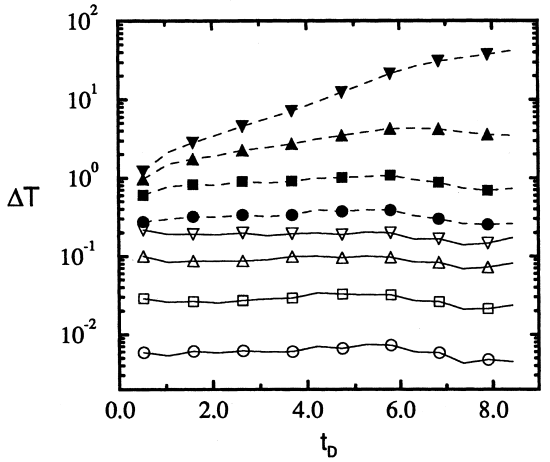

Fig. 3. Temporal variation of ΔT. Dashed lines with filled symbols represent cases with $\alpha = 4$, and solid lines with hollow symbols represent cases with $\alpha = 0.25$. Circles, squares, triangle-up and triangle-down represent $\tau_p = 1$, 2, 4, 7, respectively.

The variations of $\Delta T = \frac{\overline{\langle\langle (T'-T'_p)^2\rangle\rangle}}{\overline{\langle T'^2\rangle}}$ with α for several different values of $\frac{\tau_p}{\tau_k}$ are shown in Fig. 3. This figure indicates that despite decay of the fluid and particle temperature fields, in almost all cases ΔT attains stationary states at long times. The exception is the case with $\frac{\tau_p}{\tau_k} = 7$ and $\alpha = 4$. In this cases, ΔT grows continuously in time. Fig. 3 also shows that by increasing the particle time constant the difference between the particle and the surrounding fluid temperatures and the magnitudes of ΔT are increased (an order of magnitude increase in ΔT is observed when α increases from 0.25 to 4). The results in Fig. 3 are consistent with those reported in Ref. [17] for stationary temperature field.

The auto-correlation coefficient of the particle temperature,

$$R_T^p = \frac{\langle\langle T'_p(t_0)T'_p(t_0+\tau)\rangle\rangle}{\left[\langle\langle T'^2_p(t_0)\rangle\rangle\ \langle\langle T'^2_p(t_0+\tau)\rangle\rangle\right]^{1/2}}$$

is also dependent on α and τ_p. This is demonstrated in Fig. 4, where the temporal variation of R_T^p for different magnitudes of α and τ_p are considered. For $\alpha = 4$, as shown in Fig. 4(b), R_T^p increases significantly when τ_p increases. This is expected since heavier particles tend to keep their 'identity' better. Interestingly, for $\alpha = 0.25$, the trend is reversed and R_T^p decreases as the particle time constant increases (Fig. 4(a)). This is in contrast with the expectation that the auto-correlation of particle temperature (and particle velocity) should increase as particle inertia increases and is explained

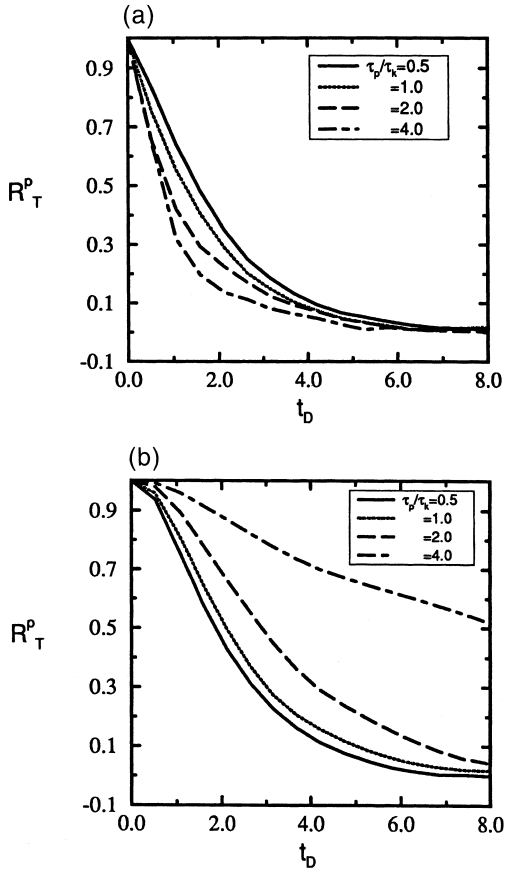

Fig. 4. Temporal variation of the auto-correlation coefficient of the particle temperature. (a) $\alpha = 0.25$; (b) $\alpha = 4$. For all cases $Pr = 0.7$.

by considering Eq. (6). For $\frac{dT_p}{dt} = 0$, the particle temperature is time invariant and $R_T^p = 1$. As the magnitude of $\frac{dT_p}{dt}$ increases, particle temperature decorrelate more from its previous values and R_T^p decreases. Eq. (6) indicates that the effect of particle time constant on $\frac{dT_p}{dt}$ (and R_T^p), is twofold. By increasing the particle time constant, R_T^p increases because $\frac{dT_p}{dt} \propto \frac{1}{\tau_p}$. At the same time, for higher values of τ_p the particle's path deviate more from the path of the surrounding fluid and $\delta T = T^* - T_p$ (or $\frac{dT_p}{dt}$) increases, which means that R_T^p decreases. The variation of δT with τ_p and α is found (not shown) to be qualitatively similar to that of the ΔT in Fig. 3. For $\alpha \leq 1$, particles rapidly respond to changes in the surrounding fluid temperature. Therefore, at early times δT is significantly increased when τ_p increases. This means that R_T^p decreases as τ_p increases (Fig. 4(a)). For $\alpha \gg 1$, particle temperature and δT vary slowly and as suggested in Fig. 3, with increasing τ_p the value of δT is much less increased than the magnitude of τ_p. Therefore, with increasing τ_p, R_T^p increases (Fig. 4(b)).

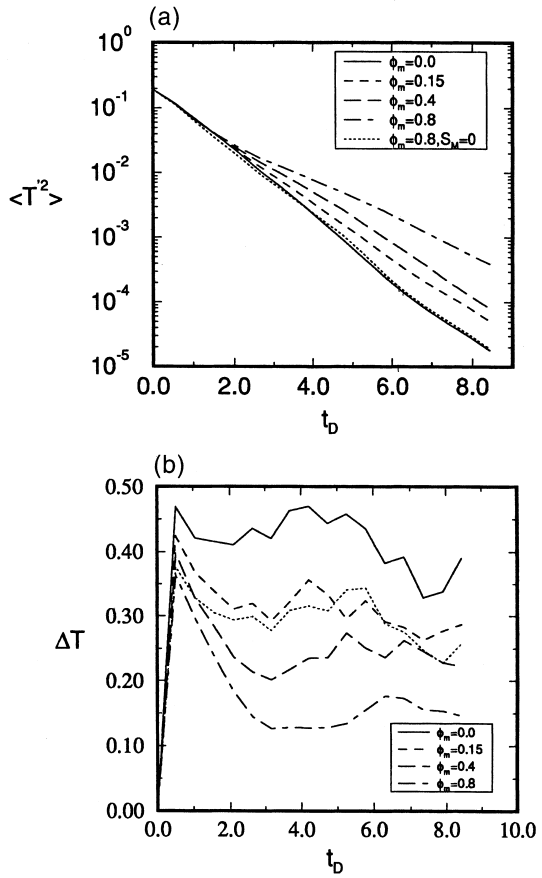

Fig. 5. Temporal variation of (a) $\langle T'^2 \rangle$, and (b) ΔT, for different mass loading ratios. For all cases $\alpha = 1$, $Pr = 0.7$ and $\tau_p = 3.6$.

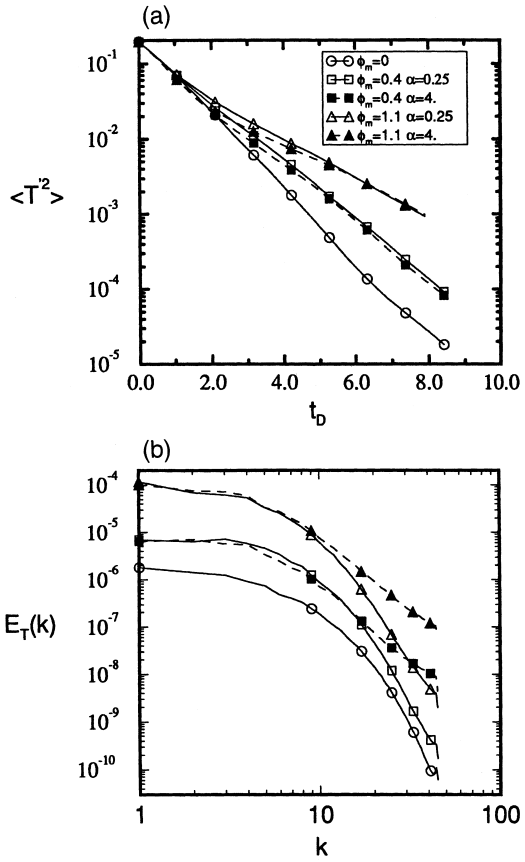

Fig. 6. Temporal variation of the fluid temperature statistics, (a) variance; (b) three-dimensional spectral density. For all cases $Pr = 0.7$.

3.2. Two-way coupling

The decay of the particle and fluid temperatures under two-way coupling condition are studied in this section. For finite particle mass loading, the fluid velocity and temperature fields are modified by the particles which results in modification of the particle velocity and temperature in a two-way coupling manner. The variation of several fluid and particle temperature statistics with mass loading ratio is considered in Figs. 5–7. Fig. 5 shows the evolution of $\langle T'^2 \rangle$ and ΔT for different ϕ_m. For all cases, $\alpha = 1$ and $Pr = 0.7$. The results in Fig. 5(a) indicate that after about two eddy turn-over times, the fluid temperature variance decay more slowly as ϕ_m increases. For $t_D < 2$, the values of the particle temperature are close to those of the surrounding fluid element due to initial conditions and the fluid temperature field is not noticeably affected by the particles. The results for particle temperature variance are similar. In contrast to $\langle T'^2 \rangle$, the long time values of ΔT are lower for higher mass loading. This is shown in Fig. 5(b) and is consistent with the results in Ref. [17]. It is also observed in Fig. 5(b) that after a significant initial overshoot, ΔT attains a nearly stationary state at long times. For the case with $\phi_m = 0.8$ and $S_M = 0$, the magnitudes of ΔT are between of those for cases with $\phi_m = 0.8$, $S_M \neq 0$ and $\phi_m = 0$, which suggests that both momentum and thermal coupling affect ΔT. However, the decay rate of the fluid (and particle) temperature variance is not significantly modified by the thermal coupling and is primarily changed due to modification of turbulent velocity field (Fig. 5(a)).

It is shown in Section 3.1 that the decay of particle temperature is dependent on the magnitude of α.

Consequently, the carrier fluid temperature is expected to be modified differently by particles as α varies. The effect of α on the decay of the fluid temperature variance for different mass loading is shown in Fig. 6(a). It is observed that at early times the rate of decay of $\langle T'^2 \rangle$ increases slightly as α increases. However, the long time values are independent of α. Our results (not shown) indicate that the dissipation

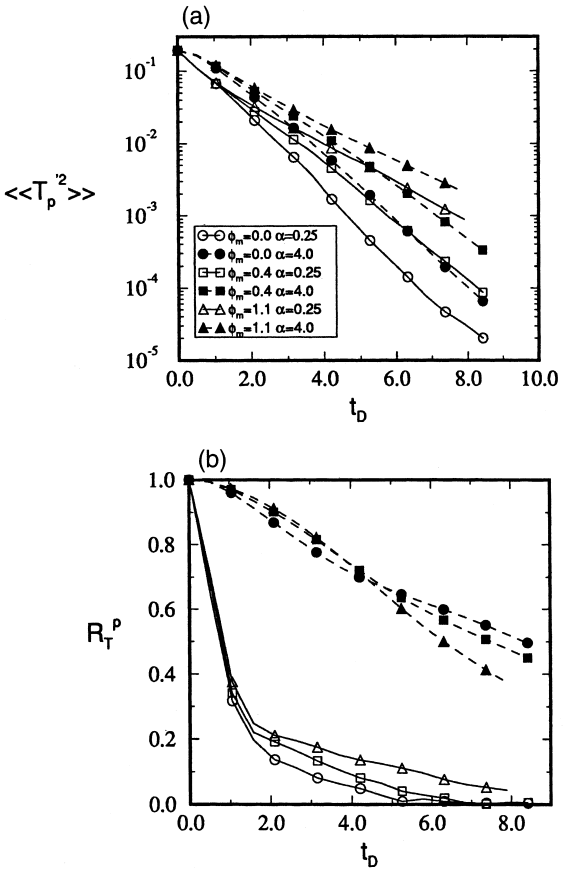

Fig. 7. Temporal variation of the particle temperature statistics, (a) variance; (b) auto-correlation coefficient. For all cases $Pr = 0.7$.

rate of the fluid temperature, ϵ_T is more significantly dependent on α. The reason is that the large scales of the fluid temperature field are affected less than the small scales by the particles. To show this explicitly, the 3D spectral density function of the fluid temperature for different values of ϕ_m and α are shown in Fig. 6(b). The results in this figure indicate that the high wavenumber values of the temperature spectra increase as the magnitude of α increases. This is, of course, more significant for higher mass loading and explains the strong dependency of ϵ_T on α. The influence of α on the low wavenumber values is relatively small. Therefore, the decay rate of the fluid temperature variance, as shown in Fig. 6(a) is not significantly dependent on the magnitude of α. The results in Fig. 6 are also consistent with those in Fig. 5 and suggest that the thermal coupling is not important as far as the decay of the large scale fluid temperature field is concerned. However, the small scale fluid temperature field is modified due to both thermal and momentum coupling.

Two-way coupling between the particles and the carrier fluid also influences the decay of the particle temperature. Fig. 7(a) shows that the values of $\langle\langle T_p'^2\rangle\rangle$ increase as the magnitudes of α and/or ϕ_m increase. However, the initial decay rate of $\langle\langle T_p'^2\rangle\rangle$ is strongly dependent on α but not so much on ϕ_m. The auto-correlation coefficient of the particle temperature also evolves differently for different magnitudes of α and ϕ_m. For the cases with $\alpha = 0.25$, as shown in Fig. 7(b), the particle temperature rapidly decorrelate from its previous values and R_T^p decreases significantly. For these cases, R_T^p increases with ϕ_m, which is consistent with the results obtained for the stationary temperature field [17]. For the cases with $\alpha = 4$, the behavior is different. For these cases R_T^p decorrelate slowly and have values larger than those for cases with $\alpha = 0.25$. Nevertheless, the effect of ϕ_m on R_T^p is similar for $t_D < 4$ and R_T^p increases with ϕ_m. At longer times, however, a reverse trend is observed and the values of the auto-correlation coefficient decrease as mass loading ratio increases.

4. Temperature decay in decaying turbulence

In this section, we investigate the general features of particle and fluid temperature statistics in decaying turbulence. While dispersion of particles in decaying turbulent flows has been extensively studied [15,29–32], to the best of our knowledge there are no experimental or numerical investigations that address the decay of the particle temperature in these flows. With the decay of turbulence, the associated length scales of the flow grow. However, for all the cases considered here the Eulerian integral length scale is less than a quarter of the box size by the end of simulations ($t_D \approx 9$). The initial velocity and temperature fluctuations of the fluid are taken from the stationary fields previously obtained by artificial forcing [17]. In all cases, $Pr = 0.7$, $\alpha = 1$, and the initial values of Re_λ, $\langle u'^2\rangle$, and $\langle T'^2\rangle$ are 48, 0.019, and 0.19, respectively. The initial velocity and temperature of the particles are the same as those of the surrounding fluid element.

The statistics of the particle velocity in decaying turbulence as observed here and by others [15] are similar to those in stationary turbulence. The statistics of the decaying temperature field are also qualitatively similar in stationary and decaying turbulence. The reason for this similarity is that in decaying turbulence the large eddies decay much slower than the small eddies. Hence, if the particle motion is controlled primarily by the large eddies, turbulence decay would not have a significant impact on dispersion of small particles. This would not be true in flows with significant gravitational drift [32]. Because of the mentioned similarity, we do not consider the results of the one-way coupled

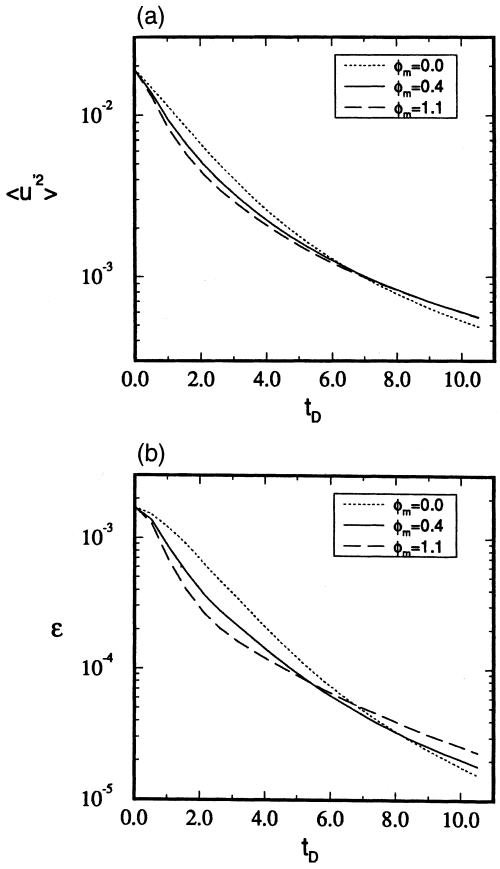

Fig. 8. Temporal variation of (a) the fluid turbulent energy; (b) the dissipation rate of the turbulent energy. For all cases $\tau_p = 3.6$, $Pr = 0.7$ and $\alpha = 1$.

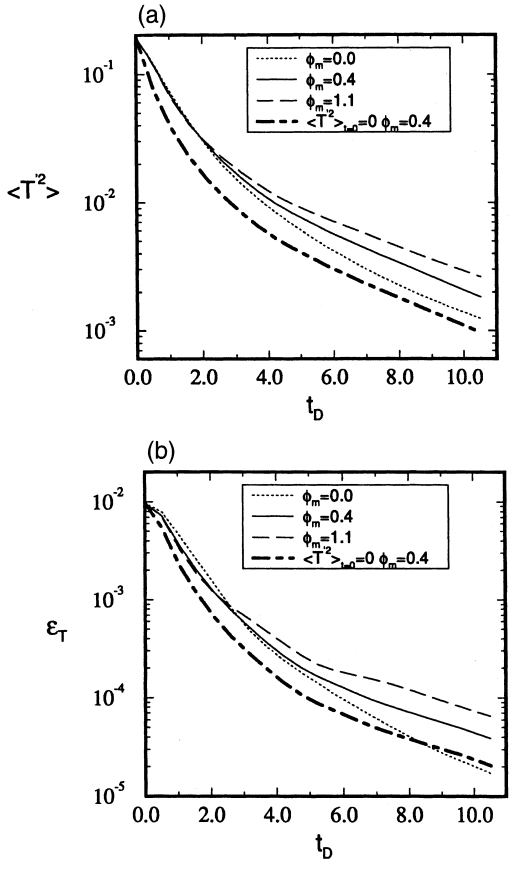

Fig. 9. Temporal variation of the fluid temperature statistics, (a) variance; (b) dissipation rate. For all cases $\tau_p = 3.6$, $Pr = 0.7$ and $\alpha = 1$.

formulation and only discuss some of the important two-way coupling results.

In Fig. 8, the decay of the turbulence energy, $\langle u'^2 \rangle$ and the total dissipation rate of turbulent energy, ϵ for different mass loading ratios are shown. It is observed that for $t_D < 6$, the turbulent energy and its dissipation rate decrease as mass loading ratio increases. At long times, the trend is reversed and both $\langle u'^2 \rangle$ and ϵ show slightly higher values for higher mass loading. The reason for the decrease of $\langle u'^2 \rangle$ during the early stages of decay, is that the rate of energy 'dissipation' by the particle drag force (ϵ_p) increases as mass loading ratio increases (not shown). The increase of ϵ_p is due to initial conditions and yields a net increase in the total dissipation rate of energy at early times. As a result, the turbulent energy decays faster for higher mass loading ratio at early times. This is consistent with the numerical results of Elghobashi and Truesdell [16] and the experimental results of Schreck and Kleis [31]. The initial increase in the rate of dissipation of turbulence energy with ϕ_m is not, however, consistent with the results of these investigations. This is attributed to the difference in the initial conditions. It is also important to mention that in the simulations of Elghobashi and Truesdell [16] the magnitude of τ_p is different in cases with different mass loading ratio.

The decay of the variance and the dissipation rate of the fluid temperature as shown in Fig. 9 is somewhat different from those of the fluid velocity. For $t_D < 2.5$, the difference between the particle temperature and the surrounding fluid temperature is small and the rate of decay of the fluid temperature variance is not affected by the particles. For $t_D > 2.5$, the decay rate decreases noticeably as mass loading ratio increases. It is also shown in Fig. 9(a) that at early times the temperature variance decays much faster when particles are initialized with no temperature fluctuations. This is understandable, since for this initialization the difference between the particle and the surrounding fluid temperatures is significant and the magnitudes of particle source term, S_H are relatively large. At long times, the rate of decay of the temperature variance is

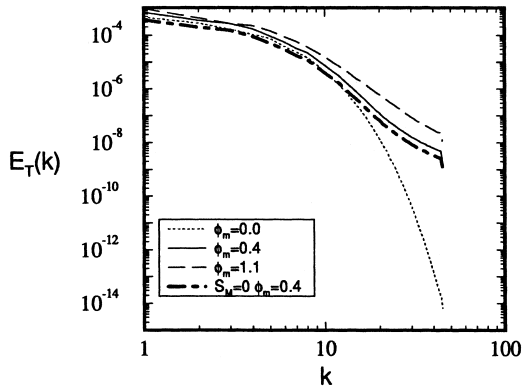

Fig. 10. The three-dimensional spectral density of the fluid temperature. For all cases $\tau_p = 3.6$, $Pr = 0.7$ and $\alpha = 1$.

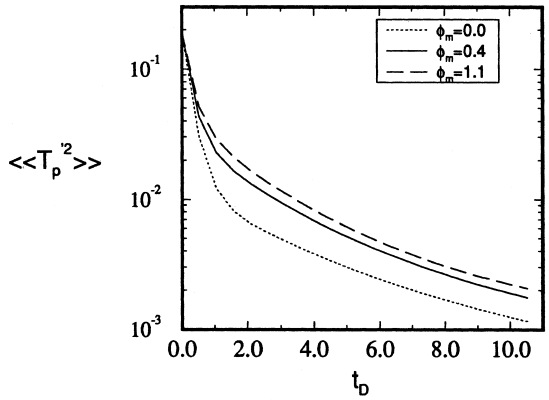

Fig. 11. Temporal variation of the particle temperature variance. For all cases $\tau_p = 3.6$, $Pr = 0.7$ and $\alpha = 1$.

independent of initial conditions. The results shown in Fig. 9(b) for ϵ_T are qualitatively similar to those for $\langle T'^2 \rangle$ in Fig. 9(a). However, the particles have more significant effect on the dissipation rate than the variance of the fluid temperature. During the initial transient time ($t_D < 2.5$), the small scales of the fluid temperature are affected by the particles and, as shown in Fig. 9(b), ϵ_T decreases slightly by increasing the mass loading ratio. For $t_D > 2.5$, similar to that of $\langle T'^2 \rangle$, the rate of decay of ϵ_T decreases noticeably with an increase in ϕ_m. Also, the early rate of decay of ϵ_T is dependent on the initial particle conditions and is the highest when particles start with no temperature fluctuations.

It is important to note that the two-way coupling effects change the particle dispersion for two different reasons. First, they enhance the interactions between the particles and the surrounding fluid. Second, they modify the structure of the turbulence. An important feature of the turbulence decay is that during the course of decay, the turbulence structure (spectra) changes significantly. Consequently, the particles are expected to have significant effects on the spectral density functions of the fluid temperature and velocity at long times. The results in Fig. 10 indicate that at $t_D = 7.4$ the high wavenumber spectral values of the temperature are relatively smaller for $\phi_m = 0$ but are significant in flows with finite mass loading and increase as ϕ_m increases. These results suggest that the effect of particles on the flow variables in decaying turbulence is scale selective and is more than that in stationary turbulence [17].

To further examine the two-way interactions between the carrier fluid and the particles, in addition to cases discussed above we have also considered several cases in which the turbulent fluctuations are generated by the particles. The initial velocity and temperature of the particles, in these cases are the same as those considered in Fig. 9. However, the initial velocity and temperature of the fluid have no turbulent fluctuations. For $\phi_m = 0$, the particles evolve in a still

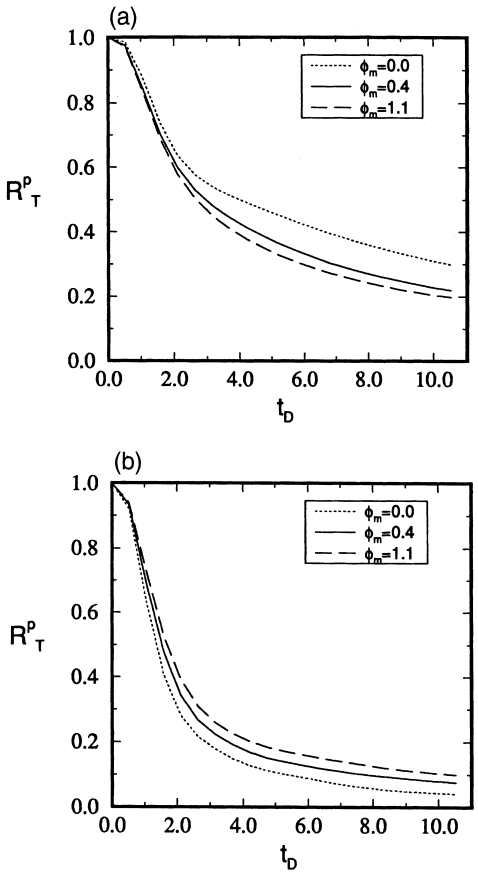

Fig. 12. Temporal variation of the particle temperature autocorrelation coefficient, (a) the fluid velocity and temperature fields have no initial turbulent fluctuations; (b) both particles and the fluid have initial turbulent fluctuations. For all cases $Pr = 0.7$ and $\alpha = 1$.

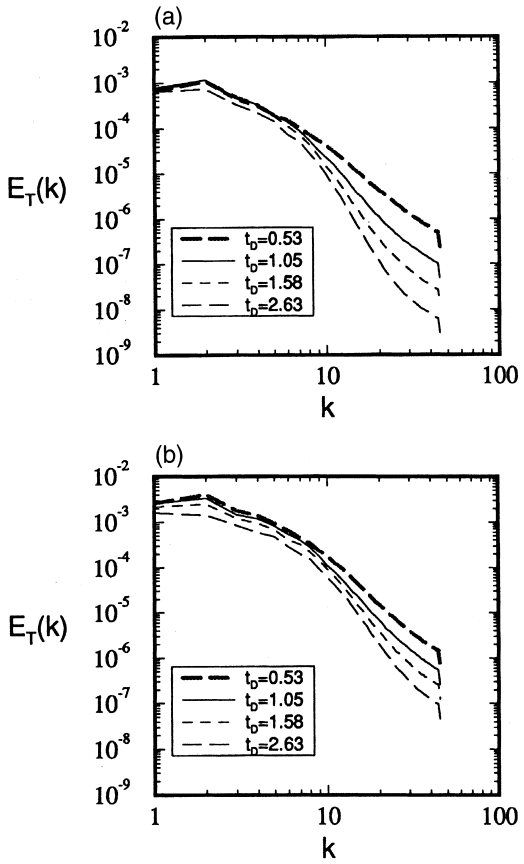

Fig. 13. The spectral density of the fluid temperature in cases with no initial fluid velocity and temperature fluctuations, (a) $\phi_m = 0.4$; (b) $\phi_m = 1.1$. For all cases $\tau_p = 3.6$, $Pr = 0.7$ and $\alpha = 1$.

fluid. For sufficiently large values of ϕ_m, the particles derive the fluid temperature and velocity fluctuations. As a result, the variance and the dissipation rate of the fluid velocity and temperature increase at early times. However, they decay later on due to viscous dissipation effects. The values of $\langle\langle v'^2\rangle\rangle$ and $\langle\langle T_p'^2\rangle\rangle$ may increase or decrease with mass loading due to two different factors. First, they may decrease because for higher mass loading, more energy is extracted from the particles by the fluid. Second, they may increase because the turbulent intensity of the fluid velocity and temperature are more significant at higher mass loading ratio and particles evolve in more 'random' environment. This means that the rms values (intensity) of the particle velocity and temperature fluctuations are higher for higher mass loading. The results shown in Fig. 11 indicate that the second factor is more important and the particle temperature intensity increases as mass loading ratio increases. Additionally, a comparison between the results in this figure with those in Fig. 9(a) (note that for cases considered in Fig. 9(a) $\langle\langle T_p'^2\rangle\rangle \approx \langle T'^2\rangle$) indicates that the particle temperature decays much faster at early times when fluid has no initial fluctuations. This is expected since by decreasing the initial fluid temperature intensity the particle and fluid temperatures differ more. The long time decay rate of the particle temperature is, however, decreased with decreasing $\langle T'^2\rangle$ and has the lowest values when the initial intensity of the fluid velocity and temperature is zero.

In the cases that the initial carrier fluid velocity and temperature fluctuations are zero, the auto-correlations of particle temperature decreases as mass loading ratio increases. This is shown in Fig. 12(a) and is opposite of the trend observed in Fig. 12(b) for the cases that the initial turbulent fluctuations are nonzero. The reason for the decrease of R_T^p is that for higher mass loading, the turbulence is stronger; therefore particles decorrelate faster in a more random environment. For the same reason, the values of R_T^p are higher when fluid has no initial turbulent fluctuations (compare Fig. 12(a) and (b)). Consistently, the long time values ($t_D \approx 10$) of the particle temperature auto-correlation coefficient in decaying turbulence (Fig. 12(b)), are finite and different for different mass loading as opposed to those in stationary turbulence [17]. These are important results and suggest that the two-way coupling effects may be different enough for different fluid and particle turbulence intensities.

The influence of the particles on different scales of the carrier fluid temperature is examined in Fig. 13, where the 3D spectral density function of the fluid temperature, $E_T(k)$ for different mass loading and at different times are shown. Initially, the fluid velocity and temperature fields have no turbulent fluctuations and $E_T(k) = 0$ for $k \neq 0$. However, Fig. 13 shows that at $t_D = 0.53$ the spectral values of the fluid temperature at all wavenumbers (length scales) are significant. Expectedly, the turbulent fluctuations are intensified more significantly and the values of $E_T(k)$ are higher for higher mass loading. At later times, the viscous dissipation effects become dominant and the fluctuations of the fluid temperature at all length scales decay, although depending on the mass loading, different scales decay differently. For $\phi_m = 0.4$, the large scales decay slowly as compared to small scales (Fig. 13(a)). The difference between the decay rate of small and large scales decrease as the mass loading ratio increases. This is evident by comparing Fig. 13(a) and (b). A comparison between these figures also indicates that for higher mass loading the large scale temperature fluctuations decay faster; opposite of the trend for small scales. The results in Fig. 13 together with those in Figs. 11 and 12 indicate that the particles have significant but different effects on different scales of the fluid temperature field, depending on their mass con-

tent, spatial distribution and velocity and temperature values.

5. Summary and conclusion

Data generated by direct numerical simulations (DNS) are used to study the decay of the particle and the fluid temperature fluctuations in two-phase isotropic turbulent flows. Both one-way and two-way coupling between the particles and the carrier fluid are considered under both stationary and decaying turbulent velocity conditions. The important parameters that characterize the temperature statistics are the particle response time (τ_p), the ratio of the specific heats (α), the Prandtl number (Pr), and the mass loading ratio (ϕ_m). The influences of these parameters on the fluid and particle temperature statistics are studied.

In stationary turbulence, the variances (intensities) of the fluid and particle temperature decay similarly for small values of αPr. Particles with large αPr values respond slowly to the decay of the fluid temperature fluctuations. Therefore, their temperature intensity remains higher than that of the fluid. The initial condition effects are also more important for higher values of αPr. Additionally, the results of our analysis indicate that the decay rates of the fluid and the particle temperature intensity decrease as mass loading ratio increases. The effects of thermal coupling on particle and fluid temperature statistics are less than the effects of momentum coupling and even for large mass loading, the long time values of the fluid temperature intensity are not significantly dependent on the magnitude of α and Pr. However, the dissipation rate of the fluid temperature is noticeably increased when αPr increases.

In one-way coupling cases ($\phi_m = 0$), the behavior of the particle temperature statistics in decaying turbulence is similar to that in stationary turbulence. This is because the particle motion is controlled primarily by the large eddies. In two-way coupling cases ($\phi_m \neq 0$), the effect of initial particle and fluid conditions on the early time values of turbulence energy and the dissipation rate of turbulence energy is significant. At long times, both of these variables show slightly higher values for higher mass loading which is consistent with the previous numerical and experimental results. Also, for $\phi_m \neq 0$, the evolution of the auto-correlation coefficient of particle temperature, R_T^p is strongly dependent on the magnitudes of α and/or Pr. For large values of αPr, with increasing the mass loading and/or the particle time constant, R_T^p increases because the particles correlate more with the carrier fluid due to momentum coupling, and also because the deviation between the particle temperature and the fluid temperature decreases due to thermal coupling. For small values of αPr, with increasing the mass loading and/or particle time constant the long time values of R_T^p decrease. In the cases that the turbulent fluctuations of the carrier fluid velocity and temperature are initially zero, the variances of the particle velocity and temperature decay more slowly as the mass loading ratio increases. However, R_T^p decreases with mass loading, opposite of the trend observed for cases in which the initial turbulence intensities of the fluid velocity and temperature are non-zero and equal to those of the particles.

References

[1] G.K. Batchelor, Diffusion in a field of homogeneous turbulence. Part II: the relative motion of particles, Proc. Phil. Soc 48 (1952) 345–362.
[2] F.N. Frenkiel, Turbulent diffusion: Mean concentration distribution in a flow field of homogeneous turbulence, Advances in Applied Mechanics 3 (1953) 61–107.
[3] A.S. Monin, A.M. Yaglom, Statistical Fluid Mechanics, vol. 2, MIT Press, Cambridge, MA, 1975.
[4] M.I. Yudine, Physical considerations on heavy-particle diffusion, Adv. Geophys 6 (1959) 185–191.
[5] G.T. Csanady, Turbulent diffusion of heavy particles in the atmosphere, J. Atmos. Sci 20 (1963) 201–208.
[6] G.M. Faeth, Mixing, transport and combustion in sprays, Prog. Energy Combust. Sci 13 (1987) 293–345.
[7] C.T. Crowe, J.N. Chung, T.R. Troutt, Particle mixing in free shear flows, Prog. Energy Combust. Sci 14 (1988) 171–194.
[8] J.K. Eaton, J.R. Fessler, Preferential concentration of particles by turbulence, Int. J. Multiphase Flow 20 (1994) 169–209.
[9] J.B. McLaughlin, Numerical computation of particles–turbulence interaction, Int. J. Multiphase Flow 20 (1994) 211–232.
[10] C.T. Crowe, T.R. Troutt, J.N. Chung, Numerical models for two-phase turbulent flows, Ann. Rev. Fluid Mech 28 (1996) 11–43.
[11] S.L. Soo, Multiphase Fluid Dynamics, Science Press/Grower Technical, Beijing/Sydney, 1990.
[12] A.A. Shraiber, L.B. Gavin, V.A. Naumov, V.P. Yatsenko, Turbulent Flows in Gas Suspensions, Hemisphere, New York, 1990.
[13] L.P. Yarin, G. Hetsroni, Turbulence intensity in dilute two-phase flows. Part II: Temperature fluctuations in particle-laden dilute flows, Int. J. Multiphase Flow 20 (1) (1994) 17–25.
[14] K.D. Squires, J.K. Eaton, Particle response and turbulence modification in isotropic turbulence, Phys. Fluids 2 (7) (1990) 1191–1203.
[15] K.D. Squires, J.K. Eaton, Measurements of particle dispersion obtained from direct numerical simulations of isotropic turbulence, J. Fluid Mech 226 (1991) 1–35.
[16] S. Elghobashi, G.C. Truesdell, On the two-way interaction between homogeneous turbulence and dispersed solid particles. Part I: Turbulence modification, Phys. Fluid 5 (7) (1993) 1790–1801.

[17] F.A. Jaberi, Temperature fluctuations in particle-laden homogeneous turbulent flows, Int. J. Heat Mass Transfer 41 (1998) 4081–4093.
[18] V. Eswaran, S.B. Pope, Direct numerical simulations of the turbulent mixing of a passive scalar, Phys. Fluids 31 (3) (1988) 506–520.
[19] V. Eswaran, S.B. Pope, An examination of forcing in direct numerical simulations of turbulence, Computers and Fluids 16 (3) (1988) 257–278.
[20] M.R. Maxey, J.J. Riley, Equation of motion for a small rigid sphere in a nomuniform flow, Phys. Fluids 26 (1983) 883–889.
[21] W.E. Ranz, W.R. Marshal, Evaporation from drops, Chem. Engng. Prog 48 (1952) 141–173.
[22] G.M. Faeth, Evaporation and combustion of sprays, Prog. Energy Combust. Sci 9 (1983) 1–76.
[23] C.T. Crowe, M.P. Sharma, D.E. Stock, The particle-source-in cell (PSI-cell) model for gas-droplet flows, J. Fluids Engineering (1977) 325–332.
[24] G.B. Wallis, One-Dimensional Two-Phase Flow, McGraw-Hill, New York, NY, 1969.
[25] P. Givi, C.K. Madnia, Spectral methods in combustion, in: T.J. Chung (Ed.), Numerical Modeling in Combustion, Taylor and Francis, New York, NY, 1993, pp. 409–452 (Chapter 8).
[26] R.M. Kerr, High-order derivative correlations and the alignment of small-scale structures in isotropic numerical turbulence, J. Fluid Mech 153 (1985) 31–58.
[27] F.A. Jaberi, R.S. Miller, C.K. Madnia, P. Givi, Non-Gaussian scalar statistics in homogeneous turbulence, J. Fluid Mech 313 (1996) 241–282.
[28] Z. Warhaft, J.L. Lumley, An experimental study of the decay of temperature fluctuations in grid-generated turbulence, J. Fluid Mech 88 (1978) 659.
[29] W.H. Snyder, J.L. Lumley, Some measurements of particle velocity autocorrelation functions in a turbulent flow, J. Fluid Mech 48 (1971) 41–47.
[30] M.R. Wells, D.E. Stock, The effects of crossing trajectories on the dispersion of particles in a turbulent flow, J. Fluid Mech 136 (1983) 31–62.
[31] S. Schreck, S.J. Kleis, Modification of grid-generated turbulence by solid particles, J. Fluid Mech 249 (1993) 665–688.
[32] F. Yeh, U. Lei, On the motion of small particles in a homogeneous isotropic turbulent flow, Phys. Fluids 3 (11) (1991) 2571–2586.